Gyro-kinetic Simulations of Internal Collapse in Reversed Magnetic Shear Tokamak

T.Matsumoto 1), H.Naitou 2), S.Tokuda 1), Y.Kishimoto 1)

1) Naka Fusion Research Establishment, Japan Atomic Energy Research Institute,
   801-1 Mukoyama, Naka-machi, Ibaraki 311-0193, Japan
2)Department of Electrical and Electronic Engineering, Yamaguchi Univ.
   2-16-1 Tokiwadai, Ube city 755-8611, Japan

email contact of main author: tmatsumo@naka.jaeri.go.jp

Abstract. The gyrokinetic particle simulation and the gyro-reduced MHD simulation are executed to clarify the kinetic modifications of the MHD phenomena in the reversed shear configuration (RSC) of a tokamak plasma. The kinetic (collisionless) double tearing modes in the RSC, which is induced not by the resistivity but by the electron inertia, are found to grow up at the Alfvén time scale by the coupling of two perturbations originated at each resonant surface. It is also found that the internal collapse occurs at the Alfvén time scale. After the internal collapse, the secondary reconnection is induced by the $m/n= 2/1$ flow. As a result of current reconcentration, a reversed shear configuration with $q < 2$ is constructed again.

1 Introduction

In fusion plasma research, the tokamak type device has a great advantage for a candidate of commercial fusion reactor. However, there are still several physical problems to be clarified until the construction and the operation of the tokamak reactor. As the plasma temperature is getting higher, besides the resistivity of plasma, kinetic effects due to the particle properties of plasma such as the electron inertia, finite Larmor radius effects of ions, and the ion Landau damping, come to play an important role on MHD modes. In particular, it is pointed out that the time scale of the magnetic reconnection becomes the order of the Alfvén time which is much faster than the resistive time scale[1, 2]. To treat the kinetic modification of the MHD modes found in the experiments, kinetic approaches beyond the resistive MHD model are inevitable.

In these days, high performance discharges with the internal transport barrier are put into practice by constituting the reversed shear configuration (RSC) in tokamaks such as JT-60U and DIII-D. However, such discharges are often suspended by the fast disruption at the beta which is lower than the critical beta predicted by the ideal MHD theory[3]. In order to clarify the kinetic effect on such phenomena, we have extended the previous gyro-kinetic particle simulation[4, 5, 6, 7] to the RSC of a cylindrical tokamak plasma, and studied the nonlinear dynamics of the internal collapses induced by the double tearing modes. We have also employed the three-field gyro-reduced MHD code [8, 9, 10, 11] for the analysis. The gyrokinetic particle simulation is more faithful to physical accuracy with the expense of a highest load to computer resources. The gyro-reduced MHD simulation, which can study the case with realistic tokamak parameters, only has a slight load to computer resources by including minimum kinetic effects. Anyway, several approaches with different orders of physical accuracy are necessary to explore the physics of the extended MHD phenomena.

This paper is organized as follows. In Section 2, we present simulation models, and describe the geometric configuration and parameters. In Section 3, the linear stability of the double tearing modes induced by the electron inertia is analyzed by the gyro-reduced MHD model. In Section 4, the nonlinear dynamics of the double tearing modes is studied by the gyro-kinetic particle model. A brief summary is given in Section 5.

2 Model and Parameters

The nonlinear gyrokinetic Vlasov-Poisson-Ampére system [12] is a basis for the gyrokinetic particle model and the gyro-reduced MHD model. The applications of the codes based on the

both models to the simulation of the $m/n = 1/1$ kinetic (collisionless) internal kink mode are reported in the previous articles [4, 5, 8]. Here, m and n are the poloidal and the longitudinal (toroidal) mode numbers, respectively. Both codes successfully simulated the fast full reconnection followed by the second phase in which the configuration of $q_0 < 1$ (q_0 is a safety factor at a magnetic axis) is reconstructed. These studies were limited to the cases of the normal shear configuration. Here, the modifications of the codes to treat the RSC are described as well as a brief summarization of the both models. The parameters used in the simulation are listed in this section.

2.1 Gyro-reduced MHD model

The gyro-reduced MHD model is derived from the moment equations of the gyrokinetic Vlasov equation. In this study, we use the three field model in the cold ion limit [10] for the electrostatic potential ϕ, z component of the vector potential A_z, and the electron density n_e. The longitudinal (toroidal) magnetic field is assumed to be in the z direction as $\boldsymbol{B} = B_0\boldsymbol{b}$ where $\boldsymbol{b}$ is the unit vector in the z direction.

The equation for n_e (the conservation law of electrons) is obtained from the zeroth order moment equation of electrons:

$$\frac{\partial n_e}{\partial t} = -\frac{\boldsymbol{b} \times \boldsymbol{\nabla}\phi}{B_0} \cdot \boldsymbol{\nabla} n_e - \frac{1}{e\mu_0}\boldsymbol{b}^* \cdot \boldsymbol{\nabla}\left(\nabla_\perp^2 A_z\right) , \tag{1}$$

where $\boldsymbol{b}^*$ is defined by $\boldsymbol{b}^* = \boldsymbol{b} + \boldsymbol{\nabla} A_z \times \boldsymbol{b}/B_0$, e is an electron charge, μ_0 is the permeability in vacuum, and $\nabla_\perp^2$ is Laplacian perpendicular to the longitudinal magnetic field. The first term on the right hand side (RHS) represents the change due to the $\boldsymbol{E} \times \boldsymbol{B}$ convection of n_e, while the second term represents the incompressibility originated from the parallel motion of electrons. Here, the Ampère's law, $\nabla_\perp^2 A_z = -\mu_0 J_e$ (J_e is the electron current along the magnetic field), is used to eliminate electron flux along the magnetic field.

The equation for A_z is the generalized Ohm's law along the magnetic field which is equivalent to the first order moment equation of electrons:

$$\frac{\partial A_z}{\partial t} = -\boldsymbol{b}^* \cdot \boldsymbol{\nabla}\phi + \delta_e^2 \frac{d}{dt}\left(\nabla_\perp^2 A_z\right) + \frac{T_e}{n_{e0}e}\boldsymbol{b}^* \cdot \boldsymbol{\nabla} n_e , \tag{2}$$

where $d/dt = \partial/\partial t + \boldsymbol{b} \times \boldsymbol{\nabla}\phi/B_0 \cdot \boldsymbol{\nabla}$ is the convective derivative, $\delta_e = c/\omega_{pe}$ with c being a speed of light in vacuum and ω_{pe} being the electron plasma angular frequency is the collisionless electron skin depth, T_e is the electron temperature, and n_{e0} is the average electron density. The second and third terms on RHS represent the kinetic effects. Without these terms, the above equation means the complete cancellation of the electrostatic and the induced electric fields along the magnetic field. The electron diamagnetic effect originates from the third term. The effect of the electron pressure gradient along the magnetic field is also included in the third term. The friction term is neglected to see the collisionless limit of the instability.

The equation for ϕ is the vortex equation which is derived by taking the convective derivative of the long wavelength limit of the gyrokinetic poisson equation including the polarization response of the ion density:

$$\frac{\partial}{\partial t}\left(\nabla_\perp^2\phi\right) = -\frac{\boldsymbol{b} \times \boldsymbol{\nabla}\phi}{B_0} \cdot \boldsymbol{\nabla}\left(\nabla_\perp^2\phi\right) - V_A^2 \boldsymbol{b}^* \cdot \boldsymbol{\nabla}\left(\nabla_\perp^2 A_z\right) , \tag{3}$$

where V_A is the Alfvén speed and the conservation law of electrons is employed.

The equation for ions are not explicitly included in the three field model although the guiding centers of ions are assumed to move only by the $\boldsymbol{E} \times \boldsymbol{B}$ drift neglecting the parallel motion along the magnetic field. The above set of equations is found to be the same as a subset of the

four field model of Hazeltine et al. [13] in certain limit [10, 11]. The inclusion of the finite ion Larmor radius effect to the above three field model is discussed in [11].

The linear stability of the kinetic internal kink mode in RSC (double tearing mode) is analyzed by using the code, GRM3F-CY, based on the three field gyro-reduced MHD model. The geometric configuration of a cylinder with a minor radius of a and a height of $L_z = 2\pi R$ (R is a major radius) surrounded by a perfectly conducting wall is assumed. A periodic boundary condition is employed in the z direction. GRM3F-CY utilizes the nonuniform mesh in the radial direction.

We selected the parameters close to the present large tokamaks: $a = 1[m]$, $R = 3[m]$, $n_{e0} = 10^{20}[m^{-3}]$, $B_0 = 5[T]$, and $T_e = 10[keV]$. For such a tokamak with deuterium discharge, $\delta_e/a = 5.32 \times 10^{-4}$ and $\rho_s/a = 2.89 \times 10^{-3}$, where ρ_s is the ion Larmor radius estimated by the electron temperature. The double tearing mode has the fine mode structure around the rational surfaces with the characteristic lengths of δ_e and ρ_s. These fine mode structure are resolved by accumulating meshes around the rational surfaces with the reasonable number of the radial mesh.

To simulate the RSC, the hollow current profile is needed. The parallel current profile is assumed to be

$$J_z = \frac{4\pi}{q_0}(1 - r^2) + \frac{0.16}{\sqrt{2\pi}d} \exp\left\{\frac{-(r - 0.4)^2}{2d^2}\right\} , \qquad (4)$$

where d is the characteristic width of the current component centered at the off-axis position at $r = 0.4$. For $d = 0.01$, the safety factor profile is shown in Fig.1(a).

2.2 Gyro-kinetic Model

We employ a gyrokinetic model[14] to simulate the double tearing modes, because it is efficient compared with the full kinetic model from a view point of the computation. In the gyrokinetic model, the characteristic time scale is larger than the ion cyclotron period. Hence, the time step size can be chosen much larger than the standard particle simulation model in which the time step size is the order of the electron plasma period.

We adopt a δf method[15] to reduce the statistical noise drastically. In the δf method the total distribution function f_σ is decomposed into equilibrium part $f_{0\sigma}$ and the perturbed part δf_σ;

$$f_\sigma(\boldsymbol{x}, p_z, t) = f_{0\sigma}(\boldsymbol{x}, p_z) + \delta f_\sigma(\boldsymbol{x}, p_z, t) , \qquad (5)$$

where σ denotes the particle species (ion and electron), p_z ($= v_z + (q_\sigma/m_\sigma)A_z$) is the longitudinal generalized momentum, q_σ is the electric charge, and m_σ is the mass. The equilibrium distribution function $f_{0\sigma}$ is assumed to be a shifted Maxwellian as

$$f_{0\sigma}(\mathbf{x}, p_z, t) = \frac{n_0}{\sqrt{2\pi}v_{te}} \exp\left\{-\frac{\left(p_z - \frac{q_\sigma}{m_\sigma}A_{z0} - v_{z0\sigma}\right)^2}{2v_{t\sigma}^2}\right\} , \qquad (6)$$

where n_0 is the equilibrium density profile, $v_{t\sigma}$ is the thermal velocity, $v_{z0\sigma}$ is the drift velocity along the magnetic field. The Ampère's law for the equilibrium part of A_z, A_{z0}, is given by the following equation:

$$\nabla_\perp^2 A_{z0} = -\mu_0 \sum_\sigma q_\sigma n_0 v_{z0\sigma} . \qquad (7)$$

It is assumed that ions do not contribute to the longitudinal current; hence, $v_{z0i} = 0$. The perturbed distribution function δf_σ is described in terms of a particle weight function w_j^σ as follows:

$$\delta f_\sigma(\boldsymbol{x}, p_z, t) = \sum_j w_j^\sigma(t) S\left[\boldsymbol{x} - \boldsymbol{x}_j^\sigma(t)\right] \delta\left[p_z - p_{zj}^\sigma(t)\right] , \qquad (8)$$

where $S\left[\boldsymbol{x} - \boldsymbol{x}_j^\sigma(t)\right]$ is a particle shape function.

The dynamics of δf is computed in a three dimensional rectangular box with the Cartesian coordinate (x, y, z). Toroidal effects are ignored for simplicity. A periodic boundary condition is adopted in the z direction. A perfect conducting wall is imposed on the x and y boundary surfaces. We assume a uniform temperature profile.

The Ampère's law for the perturbed A_z, δA_z, is written as

$$\nabla_\perp^2 \delta A_z - \sum_\sigma \left(\frac{\omega_{p\sigma}}{c}\right)^2 \delta A_z = -\mu_0 \sum_\sigma q_\sigma \left(\sum_j p_{zj}^\sigma w_j^\sigma S[\boldsymbol{x} - \boldsymbol{x}_j^\sigma]\right)$$
$$+ \sum_\sigma \left(\frac{\omega_{p\sigma}}{c}\right)^2 A_z \frac{1}{n_0}\left(\sum_j p_{zj}^\sigma S[\boldsymbol{x} - \boldsymbol{x}_j^\sigma]\right) + \sum_\sigma \left(\frac{\omega_{p\sigma}}{c}\right)^2 \frac{n_0 - \bar{n}_0}{\bar{n}_0} \delta A_z \quad, \qquad (9)$$

where $\bar{n}_0$ is the averaged density in the whole region, $\omega_{p\sigma}$ is a plasma angular frequency of species σ. The last term on RHS represents contribution from the nonuniform density profile.

The time evolution of the weight function of a particle w_j^σ is determined by the following equation:

$$\frac{dw_j^\sigma}{dt} = -\left(\frac{f_{0\sigma}}{g_{0\sigma}} - w_j^\sigma\right) \times \left\{\left[\frac{dx_j^\sigma}{dt}\left(\frac{q_\sigma}{m_\sigma}\frac{\partial A_{z0}}{\partial y} + \frac{\partial v_{z0\sigma}}{\partial y}\right) + \frac{dy_j^\sigma}{dt}\left(\frac{q_\sigma}{m_\sigma}\frac{\partial A_{z0}}{\partial y} + \frac{\partial v_{z0\sigma}}{\partial y}\right)\right]\right.$$
$$\left. \times \frac{p_{zj}^\sigma - (q_\sigma/m_\sigma)A_{z0} - v_{z0\sigma}}{2v_{t\sigma}^2} + \frac{dx_j^\sigma}{dt}\frac{\partial n_0/\partial x}{n_0} + \frac{dy_j^\sigma}{dt}\frac{\partial n_0/\partial y}{n_0} + \frac{dp_{zj}^\sigma}{dt}\frac{p_{zj}^\sigma - (q_\sigma/m_\sigma)A_{z0} - v_{z0\sigma}}{2v_{t\sigma}^2}\right\} \quad. \qquad (10)$$

Here, $g_{0\sigma}$ is the distribution function of the marker particles [15]. The second and third terms in the curly brackets on RHS represent the effect of the nonuniform equilibrium density.

The electron longitudinal drift velocity v_{z0e} is determined to produce A_{z0} which satisfies the equilibrium safety factor profile shown in Fig.1(b). Note that there are two rational surfaces for this q profile. The parameters used in the simulation are listed on Table 1. The length and the time are normalized by ρ_s and the Alfvén time $\tau_A = 1/\omega_A = L_z/V_A$, respectively. The grid size in the z-direction is selected to be 1000 times of the grid size in the poloidal plane $\Delta_\perp$. Because of the limitation of the computer resources, we are forced to use the large value of δ_e as $\delta_e = 4\rho_s = 4\Delta_\perp$.

Configuration Shape	Rectangular Box
Poloidal Mesh Width : $\Delta_\perp$	$1\ (\rho_s)$
System Size ($L_X \times L_Y \times L_Z$)	$64 \times 64 \times 32$
Number of Total Particles	$4,194,304 \times 2$
Electron Thermal Velocity	$0.25\ (V_A)$
Time Step : Δt	$2.33 \times 10^{-3}\ (L_Z/V_A)$
Skin Depth : (c/ω_{pe})	$4\ (\rho_s)$
Toroidal Mode Numbers : n	$-4 \sim +4$

Table 1 The parameters used in the gyro-kinetic particle simulation.

3 Linear Analysis of Double Tearing Modes

Linear stability of the double tearing modes in the reversed shear tokamak is analyzed by the GRM3F-CY code. The growth rate versus the minimum safety factor q_{min} is displayed in Fig.2. $m = 1, 2$, and 3 modes are shown for the broad hollow current of $d = 0.1$, while $m = 2, 3$ modes are depicted for the narrow hollow current of $d = 0.05$. To vary q_{min}, the total current is changed for the same current profile.

In the ideal MHD theory, the double tearing modes are marginally stable in the cylindrical tokamak. In the presence of the electron inertia, however, these modes are destabilized because the electron inertia acts as the effective resistivity in the Ohm's law in Eq.(2). For the $m = 2$ (or 3) mode, the growth rate has the sharp peak when q_{min} is slightly less than 2 (or 3). When q_{min}

is well below 2 (or 3), the growth rate reduces drastically but still has a finite value. The eigen mode structure for the maximum growth rates for $m = 2$ and $m = 3$ modes with $d = 0.1$ are shown in Fig.3(a) and (b), respectively. In each case, it is observed that one global mode locates between two resonant surfaces. This is characteristic of the double tearing mode in which the coupling of two perturbations originated at each resonant surface is strong. When q_{min} is well below 2(or 3), the coupling is quite weak and the growth rate is small. The growth rate for $m = 3$ is smaller than that for $m = 2$ although the difference is not so large. The growth rate for $d = 0.05$ is grater than that of $d = 0.1$ because dq/dr is large at the outer resonant surface.

The maximum growth rates for $m = 2$ are $1.2 \times 10^{-2}\omega_A$ ($d = 0.05$) and $0.41 \times 10^{-2}\omega_A$ (d=0.1). These growth rates are orders of magnitude greater than $10^{-5}\omega_A$ which is estimated by the resistive MHD model with $S = 10^{10}$ corresponding to the same parameter regime of the present study. In the real time scale, the characteristic time for the growth is of the order of a few hundred microseconds which is comparable to the time scale of the rapid growth of electron temperature perturbations observed in the experiment of RSC.

4   Nonlinear Analysis of Double Tearing Modes

4.1   Internal Collapse

The nonlinear behavior of the collisionless double tearing modes is analyzed by the gyro-kinetic particle simulation. As predicted from the linear theory, the rapid growth rate is also confirmed with the gyro-kinetic particle simulation for $\delta_e/a \sim 10^{-1}$. Figure 4 shows the electrostatic potential energy of the $m = 2$ double tearing mode in the uniform density plasma, which is decomposed in the longitudinal mode numbers n. In the linear phase ($t \leq 10$), it is obvious that the $n = 1$ (so that, $m = 2$) mode is dominant. It is also found that the growth rate of this mode is the order of Alfvén time scale ($\gamma \sim 0.52\,\omega_A$). From the view point of the computational resource, it is difficult to use the realistic tokamak parameters in the gyro-kinetic particle simulation. However, from the proportional dependence of the growth rate on the electron skin depth, the growth rate for $\delta_e/a < 10^{-3}$ is expected to be consistent with that obtained by the gyro-reduced MHD simulation.

Figure 5 shows the history of the Poincaré plots of the magnetic field lines for the $m = 2$ mode. In the linear phase, the core plasma has concentric flux surfaces and the $m = 2$ magnetic islands are located at the inner and outer $q = 2$ surfaces, as shown in (a) $t \sim 3.03$. As the mode grows, the inner islands are swept out from the central region due to the $\mathbf{E} \times \mathbf{B}$ motion induced by the $m/n = 2/1$ mode of the electrostatic potential which grows between the two resonant surfaces. At the same time, the helical flux is exchanged between two resonant surfaces, but the core plasma still remains, as shown in Fig.5(b) and(c).

At this time ($t \sim 8$), the $n = 1$ mode continues to grow up as shown in Fig.4. Then, the outer magnetic surfaces are driven into the central region. As a result of the forced reconnection, the outer magnetic surfaces combine in the central region. Therefore, the internal collapse has completed, and the equilibrium profiles are flatten inside the outer resonant surfaces. Therefore, the magnetic structure has nested flux surface, as shown in Fig.5(e). In this simulation, it is found that the internal collapse in the reversed shear tokamak can be induced at the Alfvén time scale by the double tearing mode due to the electron inertia.

4.2   Secondary Reconnection

After the internal collapse, the $n = 1$ mode does not dissipate rapidly, but keeps dominant until the end of the simulation, as shown in Fig.4. In the poloidal direction, the $m = 2$ mode is dominant as shown in Fig.6(a) ($t \sim 12.37$). This $m/n = 2/1$ mode of the electrostatic potential determines the nonlinear behavior of the double tearing mode induced by the electron inertia.

Figure 6(b) shows the perturbation of the parallel current after the internal collapse. The plasma including this current is driven into the central region again by the $\mathbf{E} \times \mathbf{B}$ motion induced by the

$m/n = 2/1$ mode. At the same time, the magnetic reconnection is forcibly induced, as shown in Fig.5(f). This is the mechanism of the secondary reconnection in the collisionless plasma. As a result of the topological change, a new core with the positive perturbation current appears, as shown in Fig.5(h). Therefore, it is found that a reversed shear configuration with $q < 2$ is constructed again due to the current re-concentration, as shown in Fig.7. If any dissipative process is induced at this time, the plasma will stay at the secondary equilibrium.

5 Summary

In order to investigate the kinetic effect on the double tearing modes in the collisionless limit, the gyro-reduced MHD model and the gyrokinetic particle model are employed. The codes based on these models are modified to treat the RSC of the cylindrical tokamak.

From the linear stability analysis by the gyro-reduced MHD model, it is found that the maximum growth rates for the $m = 2$ mode are of the order of $10^{-2}\omega_A$, which is orders of magnitude grater than $10^{-5}\omega_A$ estimated by the resistive MHD model with $S = 10^{10}$. This is because the effective resistivity due to the electron inertia is larger than the plasma resistivity in high temperature plasma. In the real time scale, the characteristic time for the growth is found to be of the order of a few hundred microseconds which is comparable to the time scale of the rapid growth of electron temperature perturbations observed in the experiment of RSC.

From the nonlinear simulation by the gyro-kinetic particle model, it is clarified that the internal collapse can be induced at the Alfvén time scale as a result of the nonlinear evolution of the kinetic (collisionless) double tearing mode. After the internal collapse, the $m/n = 2/1$ of the electrostatic potential mode is still dominant. Then, the secondary magnetic reconnection is forcibly induced by the $\mathbf{E} \times \mathbf{B}$ motion. As a result of the current re-concentration, it is also found that a reversed shear configuration with $q < 2$ is constructed again. If any dissipative process is induced at this time, the plasma is expected to stay at the secondary equilibrium.

References

[1] J.A. Wesson, Nuclear Fusion **30** (1990) 2545.

[2] D. Biskamp, J.F. Drake, Phys. Rev. Lett. **73** (1994) 971.

[3] T. Fujita, T. Hatae, T. Oikawa, et.al., Nuclear Fusion **38** (1998) 207.

[4] H. Naitou, K. Tsuda, W.W. Lee, R.D. Sydora, Phys. Plasmas **2** (1995) 4257.

[5] H. Naitou, T. Sonoda, S. Tokuda, V.K. Decyk, J. Plasma and Fusion Research **72** (1996) 259.

[6] T. Matsumoto, S. Tokuda, Y. Kishimoto, T. Takizuka, H. Naitou, J. Plasma and Fusion Res. **75** (1999) 1188.

[7] T. Matsumoto, S. Tokuda, Y. Kishimoto, T. Takizuka, H. Naitou, J. Plasma and Fusion Res. Series Vol.2, (1999) 97.

[8] H. Naitou, H. Kitagawa, S. Tokuda, J. Plasma and Fusion Res. **73** (1997) 174.

[9] H. Naitou, T. Kobayashi, S. Tokuda, J. Plasma Phys. **61** (1999) 543.

[10] H. Naitou, T. Kobayashi, T. Kuramoto, S. Tokuda, T. Matsumoto, J. Plasma and Fusion Res. SERIES, Vol.2, (1999) 259.

[11] H. Naitou, T. Kuramoto, T. Kobayashi, M. Yagi, S. Tokuda, T. Matsumoto, J. Plasma and Fusion Res. **76** (2000) 778.

[12] T.S. Hahm, W.W. Lee, A. Brizard, Phys. Fluids **31** (1988) 1940.

[13] R.D. Hazeltine, C.T. Hsu, J. Morrison, Phys. Fluids **30** (1987) 3204.

[14] W.W. Lee, Phys. Fluids **26** 556 (1983).

[15] S.E. Parker, W.W. Lee, Phys. Fluids **B5** 77 (1993).
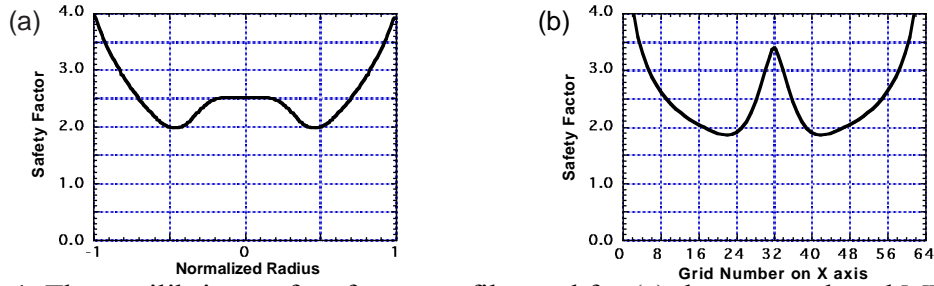
Figure 1 The equilibrium safety factor profile used for (a) the gyro-reduced MHD simulation (x/a= -1~ +1) and (b) the gyro-kinetic particle simulation (on the y=32 line).
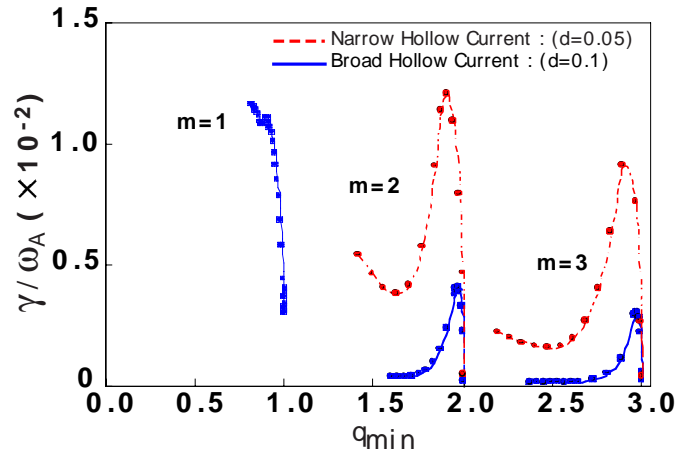

Figure 2 The q_{min} dependence of the growth rate of m=1, 2 and 3 kinetic double tearing modes is shown, where the solid lines indicate the growth rate with a broad hollow current (d=0.1) and the dashed lines mean those with a narrow hollow current (d=0.05).
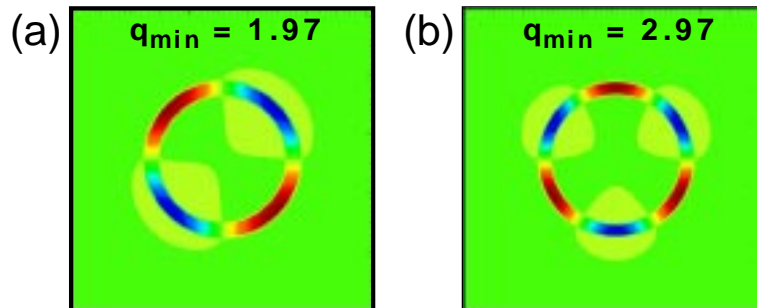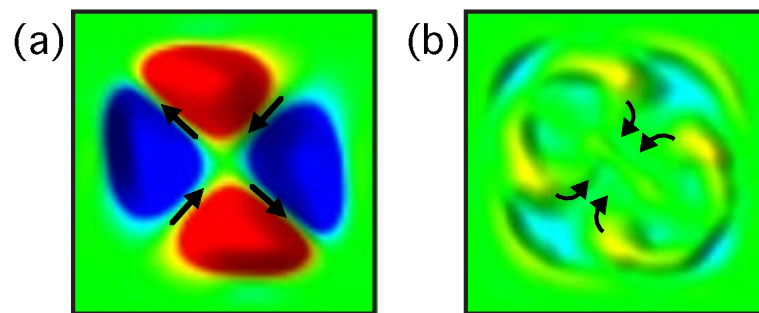

Figure 3 The electrostatic potential structure of (a) the m=2 mode for q_{min} = 1.97, and (b) the m=3 mode for q_{min} = 2.97. The mode structure locates between two resonant surfaces.
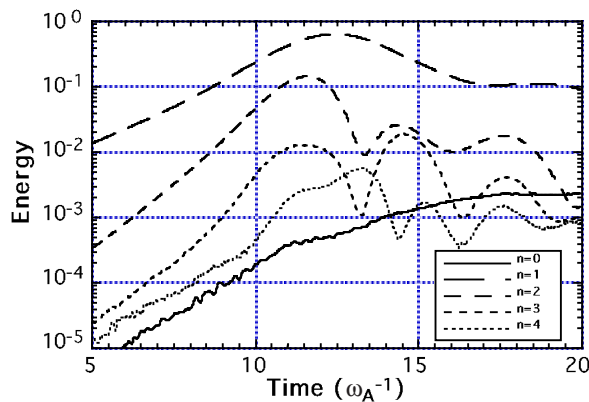

Figure 4 The time evolution of the electrostatic potential energy decomposed in the longitudinal (toroidal) mode number n.
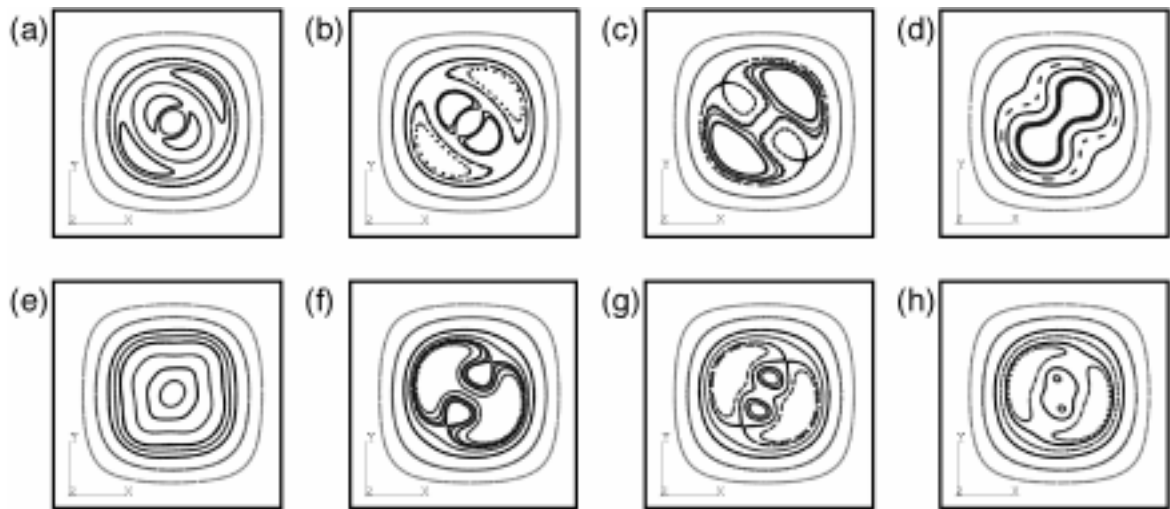
Figure 5 Poincare plots of the nonlinear simulation at (a)t=3.03, (b)t=5.13, (c)t=7.94, (d)t=10.50, (e)t=12.37, (f)t=17.97, (g)t=18.67, and (h)t=19.60.

Figure 6 The contours of (a) the electrostatic potential and (b) the perturbation of the parallel current just after the internal collapse (t=12.37), where the arrows mean the **ExB** flow and the movement of the parallel current peak, respectively.
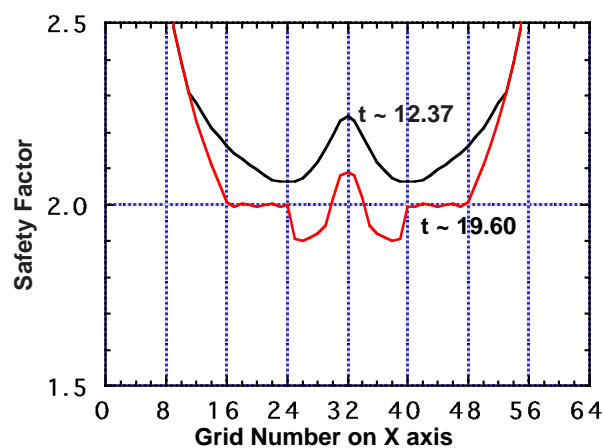
Figure 7 The safety factor profile on the y=32 line (a) just after the full reconnection (t=12.37) and (b) in the secondary reconnection (t=19.60).